

Extended Charge Carrier Lifetimes in Hierarchical Donor–Acceptor Supramolecular Polymer Films

Carmen X. Guzman,[†] Rafael M. Krick Calderon,[†] Zhong Li,[†] Shiori Yamazaki,[†] Samuel R. Peurifoy,[†] Chengchen Guo,[‡] Stephen K. Davidowski,[‡] Mercedes M. A. Mazza,[†] Xu Han,[†] Gregory Holland,[§] Amy M. Scott,^{*,†} and Adam B. Braunschweig^{*,†}

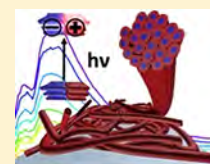
[†]Department of Chemistry, University of Miami, Coral Gables, Florida 33146, United States

[‡]Department of Chemistry and Biochemistry, Magnetic Resonance Research Center, Arizona State University, Tempe, Arizona 85287-1604, United States

[§]Department of Chemistry and Biochemistry, San Diego State University, 5500 Campanile Drive, San Diego, California 92182-1030, United States

S Supporting Information

ABSTRACT: We report that supramolecular polymer films composed of a 2:1 mixture of monodiamidopyridine diketopyrrolopyrrole (DPP) electron donors and perylene bisdiimide (PDI) electron acceptors undergo photoinduced charge transfer in the solid state. Film formation is guided by complementary noncovalent interactions programmed into the molecular components, resulting in a film architecture comprised of polymer wires with order across the molecular-to-macroscopic continuum. Using ultrafast transient absorption spectroscopy, we show that recombination lifetimes increase 1000-fold compared to the same supramolecular polymers in solution. Supramolecular donor–acceptor polymer films, such as these, that are designed by considering structure and electron transfer dynamics synergistically could lead to breakthroughs in organic optoelectronics.



INTRODUCTION

Significant efforts have been devoted toward improving the performance of small molecule organic photovoltaics (OPVs);^{1–4} however, challenges still remain with regard to understanding, controlling, and ultimately optimizing the photon-to-current conversion within the photoactive layer. Natural photosynthetic processes that efficiently convert sunlight to fuel rely upon precisely positioned assemblies of photofunctional chromophores for light harvesting, charge separation, and catalysis.⁵ Light conversion in the reaction center involves the synergistic combination of superstructure and ultrafast electron transfer to form long-lived radical pairs.^{6,7} The near unity conversion of light to chemical energy in the reaction center is a compelling model for future solar technologies⁸ and has inspired the design of organic materials for artificial photosynthesis.^{9–11} Similar to the reaction center, the photoactive layers of OPVs require appropriately matched donor and acceptor frontier molecular orbital levels and electronic coupling that enable rapid charge generation, and the resulting films must also possess multilength scale order for charge migration through the films.^{12,13} Approaches for designing these materials must consider ease of preparation, solar spectrum absorption, electron transfer dynamics, and film order together to achieve efficient charge generation.

Supramolecular polymers are a promising class of materials that could potentially be used for preparing organized films that undergo photoinduced charge separation. Supramolecular polymers are macromolecules whose monomeric repeat units are held together by noncovalent bonds, and their noteworthy

characteristics include assembly from easy-to-prepare small molecules, hierarchical structure, and stimuli responsiveness.^{14–19} Several supramolecular polymer systems have been explored in the context of photoinduced charge separation in solution^{20–23} and the solid-state,^{24–27} including a system we developed composed of a monodiamidopyridine diketopyrrolopyrrole (mDPP) electron donor and a perylene bisimide (PDI) electron acceptor²⁸ that assembles into 2:1 mDPP:PDI helical supramolecular polymers (Figure 1a) as a result of cooperative hierarchical assembly involving $\pi\cdots\pi$ stacking and H-bonding.²⁹ In solution, this mDPP:PDI supramolecular polymer undergoes ultrafast photoinduced charge separation into mDPP^{•+}:PDI^{•-} followed by a recombination $\tau_{CR} = 33$ ps. Thus, we sought to investigate whether this emergent photophysical property—photoinduced charge separation—observed when the donor–acceptor superstructures formed in solution could be translated to the solid state. The challenge however is that the structures of supramolecular polymers that arise in solution and that produce the desirable emergent properties are not always maintained in thin films, and the effect of the condensed phase on photophysical properties are difficult to anticipate. Herein we report how mDPP:PDI supramolecular polymer structure is maintained in the solid state with order at the molecular and micrometer length scales, leading to photoinduced charge separated states that persist

Received: April 17, 2015

Revised: July 20, 2015

Published: July 21, 2015

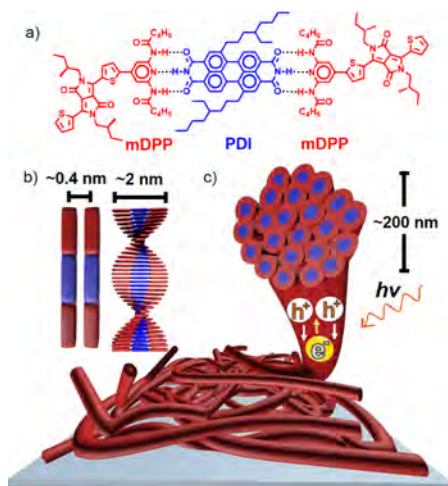


Figure 1. (a) Chiral mDPP donor (red) and the PDI acceptor (blue) forming 2:1 aggregates as a result of H-bonding. (b) π -Stacking orthogonal to the H-bonding creates donor–acceptor supramolecular polymers with helical chirality. (c) Drop-casting of a 2:1 mDPP:PDI solution results in films composed of hierarchical ropes whose fibers are the chiral supramolecular polymers that contain π -channels for transport following photoinduced charge separation.

1000-fold longer in the solid-state than in solution. This finding is significant because charge carrier lifetime is directly related to the ability to collect and use the resulting charges. In this communication we report how mDPP:PDI films were prepared, how their solid-state structures were characterized, and the electron transfer kinetics that dominate upon ordered-thin film formation to produce remarkably long-lived charge carriers.

FILM CHARACTERIZATION

Our first aim was to prepare films of the supramolecular polymers and determine whether the noncovalent bonding and helical structure observed in solution persisted in the solid-state, and extensive details of the structural characterization of the thin films are provided in the [Supporting Information](#). Films of the donor, acceptor, and supramolecular polymer were formed by drop-casting from hot toluene solutions, and upon solvent evaporation the mDPP formed microcrystals, the PDI formed powders, and the 2:1 mDPP:PDI solution formed hierarchical films with order across the molecular-to-micrometer continuum. Previous studies have shown the need to aggregate data from multiple characterization methods to arrive at accurate film structures for noncovalently organized donor–acceptor films,^{25,27–30} so we combined data from multiple solid-state analytical techniques that probe structure at the supramolecular, nanometer, and micrometer scales and compared them with solution data to arrive at a structure for the 2:1 film that consists of a dense mat of ropes that are bundles of 2:1 mDPP:PDI chiral helices, each of which has three parallel π -channels that propagate along the helical axis ([Figure 1b](#)). Attenuated total reflectance infrared (ATR-IR) and multidimensional ^{13}C solid-state nuclear-magnetic resonance (ssNMR) spectroscopies confirmed the triple H-bonding between the diamidopyridine (DAP) group on the mDPP and the diimide group on the PDI. The ATR-IR spectrum of the mDPP film ([Figure 2a](#)) displays two distinct N–H stretch peaks, a sharp peak at 3392 cm^{-1} , and a broad peak at 3276 cm^{-1} , which are attributed to amide protons that are not and are involved in H-bonding with the carbonyls of DAP groups on adjacent mDPPs, respectively, suggesting the mDPP adopts similar supramolecular H-bonding in the films as in the crystal structure of the previously reported²⁸ achiral mDPP ([Figure](#)

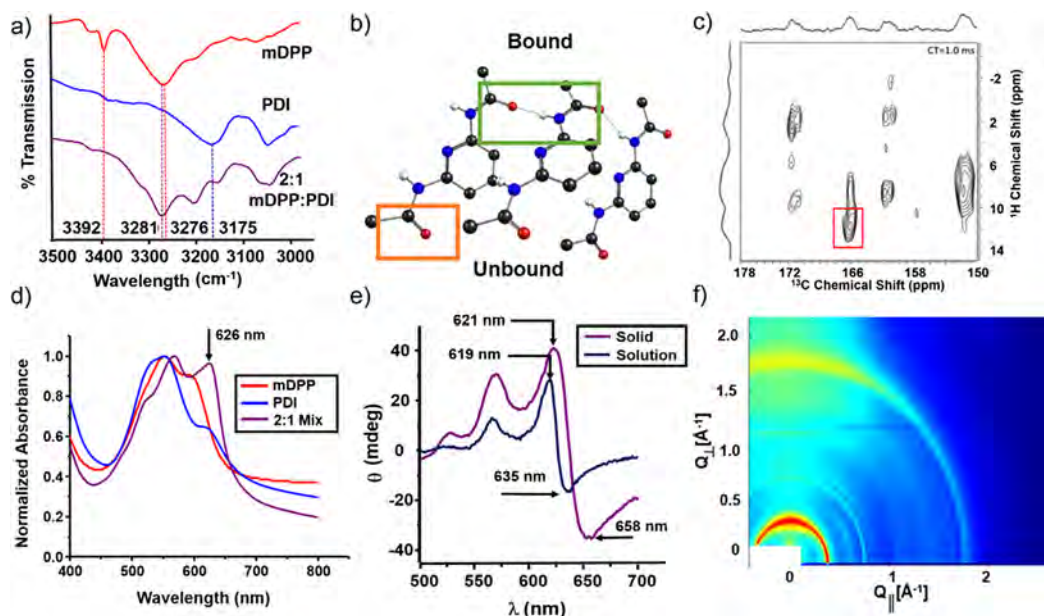


Figure 2. (a) ATR-IR spectra of films of mDPP (red), PDI (blue), and 2:1 mixture (purple). (b) Diamidopyridine regions taken from the crystal structure of achiral mDPP. Orange and green squares highlight the amide protons that are not and are participating in H-bonds, respectively. Color of atoms: Carbon, black; nitrogen, blue; oxygen, red; and hydrogen, white. Highlighted are the unbound and bound amines of the DAP group. (c) HETCOR solid-state ^{13}C NMR of the 2:1 mDPP:PDI mixture. The box indicates the amide proton of mDPP involved in H-bonding with the PDI. (d) Film UV–vis spectra of mDPP (red), PDI (blue), and 2:1 mixture (purple). Highlighted is the charge transfer peak at 626 nm that emerges upon superstructure formation. (e) Overlaid CD spectrum of the 2:1 mixture in solution (navy blue) and in the film (purple). (f) GIWAXS of the 2:1 mDPP:PDI mixture.

2b). The ATR-IR spectrum of the 2:1 mDPP:PDI film has only a single broad peak at 3281 cm^{-1} in the N–H stretch region, which suggests that all DAP amide protons in the film are involved in H-bonding, and the simplest explanation consistent with this data is that both DAP amides H-bond with the PDI carbonyls. This analysis is further supported by ssNMR. The ^1H resonance at 11.7 ppm that appears in the 2:1 mDPP:PDI mixture is assigned to amide protons of PDI forming strong H-bonding with the pyridyl functional group of mDPP (Figure S3). The ^1H – ^1H dipolar DQ/SQ NMR spectra (Figure S6) show that the strong H-bonding resonance at 11.7 ppm correlates to the amide protons of mDPP. The amide proton of PDI correlates to the DAP amide protons of mDPP, which is consistent with the two types of H-bonding that are expected in the superstructure. The $^1\text{H} \rightarrow ^{13}\text{C}$ two-dimensional (2D) heteronuclear correlation (HETCOR) (Figure 2c) shows a correlation between the strong H-bonding site ^1H resonance in the 2:1 mDPP:PDI and a ^{13}C resonance in the carbonyl region at 166 ppm.

The $\pi\cdots\pi$ stacking and chirality of the films was interrogated by UV–vis and circular dichroism (CD) spectroscopies, and taken together these data confirm that the emergent helical chirality observed previously^{28,29} in 2:1 mDPP:PDI solutions is maintained in the drop-cast films. The UV–vis spectrum of the 2:1 mDPP:PDI film shows considerable vibronic sharpening compared to the individual components, and in similar systems^{24,25} this phenomenon has been ascribed to ordering resulting from $\pi\cdots\pi$ stacking. In the 2:1 film, a characteristic charge transfer peak appears at 626 nm (Figures 2d and S1), and this peak is similar to the charge transfer peak at 622 nm that appears in solution^{28,29} following formation of donor–acceptor supramolecular polymers composed of parallel channels of mDPP and PDI. This self-stacking of PDI^{31–33} and mDPP³⁴ in the solid-state is consistent with previous literature reports, and the self-segregation likely arises because self-stacking maximizes the π -surface overlap. Further evidence for this helical structure is provided by similarities between the CD spectrum of the 2:1 mDPP:PDI superstructures in solution and the solid-state, which both display bisignated Cotton effects (the signature of helical dyes^{35–37}) with nearly identical shapes and peak positions (Figure 2e). Importantly, the CD spectra of the chiral mDPP present no significant Cotton effect either in solution or in films;²⁸ rather helical chirality only emerges upon cooperative assembly of the donor–acceptor supramolecular polymers. Thus, on the nanometer scale, these spectroscopic data are consistent with a film structure composed of helical 2:1 mDPP:PDI helices held together by homo $\pi\cdots\pi$ stacking along the helix axis and orthogonal triple H-bonding.

Order on different length scales is the hallmark of biological materials,^{38–40} and in the context of light harvesting in photosynthetic systems, order on the nanometer scale directs charge generation, and long-distance order prevents charge recombination. To investigate whether hierarchical order was present in the 2:1 mDPP:PDI supramolecular polymer films, the micrometer-scale structure of the different films was investigated by polarized optical microscopy (POM), atomic force microscopy (AFM), scanning electron microscopy (SEM), and grazing-incidence wide-angle X-ray scattering (GIWAXS), AFM topographical imaging (Figure 3a,b), and SEM (Figure 3c,d) of the 2:1 mDPP:PDI film. These studies revealed a dense tangle of wires that are each several micrometers in length, and the height of the film was $0.32 \pm 0.054\ \mu\text{m}$ with individual wires ranging in diameter from ~ 50

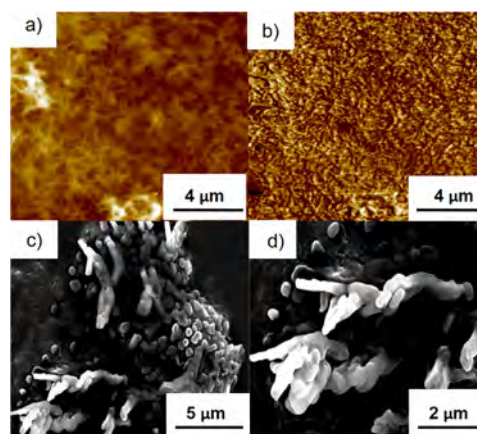


Figure 3. (a) AFM topography image of 2:1 mDPP:PDI mixture on glass. (b) AFM phase image of 2:1 mDPP:PDI mixture on film. (c, d) SEM images at different magnifications of a bundle of supramolecular polymer wires.

to $\sim 200\text{ nm}$. POM images (Figures S23 and S24) confirmed that the mDPP formed crystals with lengths of $\sim 100\ \mu\text{m}$, the PDI formed powders, and the 2:1 mDPP:PDI mixture formed a relatively homogeneous film without evidence of grain structure or microdomains. The GIWAXS data provide further evidence of microscale order and preferential orientation in the three films. The strong reflections along Q_{\perp} at 0.395 (1.589 nm) for the mDPP correspond to the lamellar spacing,⁴¹ and the PDI peak at $0.328\ \text{Å}^{-1}$ (1.923 nm) is one of several peaks in the correct region of the spectrum that indicates lamellar assembly. The peaks at 1.482 (0.424 nm) (mDPP)²⁴ and $1.564\ \text{Å}^{-1}$ (0.401 nm) (PDI)⁴² along Q_{\perp} are consistent with other PDI GIWAXS data²⁴ and correspond to the $\pi\cdots\pi$ stacking (Figure S16, Table S3), suggesting that these dyes are arranged with the π -channels propagating parallel to the surface (Figure S21). The GIWAXS of the 2:1 mDPP:PDI films differs markedly. By comparing the GIWAXS data, a few conclusions can be drawn about the mDPP:PDI supramolecular polymer films. First, the absence of peaks in the mixed films between 1.162 and $1.181\ \text{Å}^{-1}$ that are prominent in the individual components confirms that this film is indeed composed of a new superstructure rather than just domains of individual components. Second, the radial nature of the peaks indicates there is no preferential orientation of the crystallites relative to the surface normal, although the $\pi\cdots\pi$ stacking peak at $1.8\ \text{Å}^{-1}$ is stronger along Q_{\perp} , suggesting a modest preference for propagation of the π -channels along the surface normal (Figure 2f). A more thorough analysis of the GIWAXS data will be provided in forthcoming publications. This hierarchical structure, whereby the solid-state structure is composed of a small fibers coiled into larger ropes, is consistent with all thin film characterization data and is remarkably similar to that arrived at with a similar donor–acceptor system that uses PDI to bridge two oligo(*p*-phenylenevinylene) units.²⁵

■ TRANSIENT ABSORPTION SPECTROSCOPY

To compare the photoinduced charge transfer processes of the mDPP-PDI films to those previously reported^{28,29} for solution aggregates, a brief description of the femtosecond (fs) and nanosecond (ns) transient absorption (TA) on the individual compounds and on the 2:1 mDPP:PDI mixture in toluene is provided. Photoexcitation of solutions of mDPP and PDI in toluene (Figure S26A,B), results in the appearance of ground state bleaching from 523–594 nm with corresponding positive

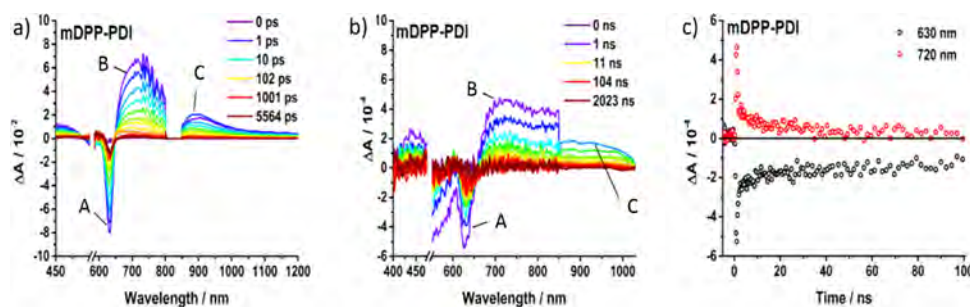


Figure 4. (a) fs-TA spectra and (b) ns-TA spectra of films of 2:1 mDPP:PDI mixture upon 500 nm laser excitation. (c) Time-absorption profiles of the 2:1 mDPP:PDI mixture (4.5–5.5 ns delay) film at 630 and 720 nm illustrating the charge recombination.

excited states features between 700 and 800 nm and lifetimes around 2–5 ns. Ground state bands observed at 650 and 578 nm are from stimulated emission for both mDPP and PDI, respectively. Upon assembly of mDPP and PDI into a 2:1 mixture (83 μM /42 μM), a new, negative feature at 622 nm is observed, which is not present in the individual electronic absorption spectra. We have previously shown from UV-vis data^{28,29} that the peak at 622 nm appears as a result of aggregation, and calculations indicate the energy of this peak corresponds to a charge transfer band using the Weller treatment. In toluene, the charge separation energy (ΔG_{CS}) is estimated to be 2.0 eV (620 nm), and this peak appears in both solution aggregates (622 nm) and the supramolecular polymer film presented here (626 nm). The ground state recovery of the charge transfer band at 622 nm follows the charge recombination of mDPP^{•+} and PDI^{•-} radical ions previously reported by us²⁹ and others,²⁴ with both ions absorbing broadly from 700–800 nm. Individual kinetics fit as a sum of exponentials of the ground state charge transfer band bleach at 622 nm and the radical ions at 722 nm are identical. The dynamics are biexponential with a fast component of 33.1 ± 0.5 ps (76%) from charge recombination, and a slow component of 3.74 ± 0.18 ns (24%) matching those lifetimes of the individual chromophore excited state lifetimes. Further experiments were performed to disrupt H-bonding in the aggregates using 5% DMSO (Figure S26D). In this case, the TA within the 2:1 DPP:PDI mixture resembles a linear combination of the individual compounds with the 622 nm ground state bleach noticeably absent from the spectra and a significant decrease in intensity of the broad absorption from 700–800 nm.

fs-TA and ns-TA were used to investigate photoinduced charge transfer dynamics in air-free films of mDPP, PDI, and the 2:1 mDPP:PDI mixture. Ultrafast excited state kinetics and spectra were first examined for ¹*mDPP and ¹*PDI as a function of pump energy density and wavelength, and those kinetics were fit as a sum of exponentials (Table S4 and Figure S30). Laser irradiation of the PDI film at 500 nm produces peaks corresponding to ¹*PDI transitions from 620 to 1400 nm (Figure S32A), with maxima at [a] 710 and 909 nm, consistent with the PDI excited state energies. The ¹*PDI deactivates multiexponentially, with lifetimes contributions of ~ 1 ps (72%), assigned to excited state annihilation, 41 ps (15%), and a long-lived component > 6 ns that are similar to previously reported excited state absorption decays of other PDI-containing films.^{29,43} The mDPP films that were photoexcited at 500 nm produce ¹*mDPP features at 450 nm and [b] 606 nm along with a broad absorption from 640 to 1200 nm, with maxima at [d] 707 nm and [e] 885 nm (Figure S32B) that are assigned to singlet excited state transitions (S_1 – S_n). Negative

features between 480 and 595 nm correspond to ground state bleach, and stimulated emission at [c] 630 nm –650 nm appears on the picosecond time scale. The kinetics at [c]–[e] follow identical multiexponential decays, with average lifetimes of ~ 3 ps (37%), 48 ps (35%), and 306 ps (26%) and a measurable long-lived component that persists on the nanosecond and microsecond time scales (Table S4). The multiexponential decay of the ~ 2 ps component can be rationalized by ¹*mDPP annihilation, whose contribution decreases with decreasing pump energies (Figure S30).

Upon photoexcitation of the 2:1 mDPP:PDI mixture film at 500 nm, positive features at ~ 450 nm along with a broad transient from 650 to 1200 nm (Figure 4a) with maxima at [B] 733 nm and [C] 902 nm form within the instrument response time (~ 70 fs). These transients are accompanied by a depletion of the charge transfer band [A] at 626 nm (Figure 4a). All positive signals at early times in the femtosecond transient absorption spectrum are nearly identical to spectroelectrochemical film data collected for the mDPP^{•+} and PDI^{•-} radical ions, confirming that charge separation occurs in the donor-acceptor films as it does in solution (Figures S25, S26, and S28). During the time window observable with the femtosecond transient absorption setup, these kinetics decay multiexponentially (Figure 4 and Table S4). Similar results were obtained upon photoexcitation at 625 nm (Table S4 and Figures S26 and S27). In the 2:1 mDPP:PDI films, the slowest charge recombination takes place within 32 ns, which was determined by monitoring the transient absorption features across the visible and NIR spectrum (Figure 4b). Interestingly, we observe an identical ~ 33 ps charge recombination component matching solution aggregate dynamics, with an amplitude reduced by half in the supramolecular polymer films, indicating that ion pairs are able to overcome coulomb energy to form free charge carriers in the condensed phase.⁴⁴ This slowest recombination is approximately 1000-fold greater than the 33 ps lifetime observed in the solution aggregates. However, the ground state bleach at the charge-transfer band at 626 nm is not fully recovered, and an appreciable amount ($\sim 5\%$) of this signal is left after 32 ns that was not observed in solution (Figure 4c) that suggests long-lived triplet states may be formed from either individual mDPP or PDI or as a triplet excited state produced from photogenerated triplet radical pairs (Figure S28). Previous studies in related H-bonded^{22,25,45} and covalent systems²⁴ have shown that the relative orientation of donor and acceptor components contributes to the emergent photophysics of similar systems, where charge separation occurs within 2–3 ps through the H-bond and charge separation through cofacial interactions occurs on the fs time scale. From the spectroscopic analysis, we were able to

construct a Jablonski diagram (Figure 5) describing the various photophysical processes occurring in these materials comparing

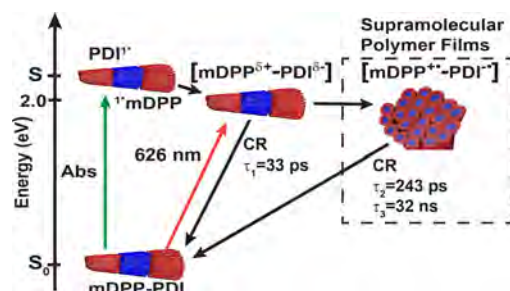


Figure 5. Jablonski diagram comparing the photoinduced charge recombination (CR) pathways of mDPP:PDI in solution aggregates to those observed in supramolecular polymer films. Increased yields of free charges with extended lifetimes are observed in the films as charge delocalization increases.

solution aggregates with supramolecular polymer films following photoexcitation. These data suggest that in the mDPP-PDI supramolecular polymers studied herein, charge separation occurs through cofacial interactions, and this interpretation is further supported by ground-state charge transfer absorption band at 626 nm.²⁹ The increased recombination lifetimes observed in the mDPP:PDI films ($\tau_2 = 243$ ps and $\tau_3 = 32$ ns) likely arise from charge delocalization through the π -channels in the fibers or hopping of charges between the fibers in the condensed phase,⁴⁶ and both experimental and theoretical efforts are being made to resolve this source of this significant lifetime increase. The trends observed in the spectroscopic data of the 2:1 mDPP:PDI films are similar to the those observed for a covalently linked PDI-DPP-PDI system reported by Wasielewski et al.²⁴ following solvent annealing. Like them we observe a significant increase in charge carrier lifetimes in moving from solution to films, likely because of the ability of free charge carriers to move through the π -channels upon ordering.

In conclusion, TA was used to study charge dynamics in films composed of an electron rich mDPP donor and an electron poor PDI acceptor that coassemble into hierarchically ordered supramolecular polymers as a result of multiple noncovalent interactions operating in concert, and this proposed structure is consistent with all experimental data. TA results reveal that charge carrier lifetimes increase 1000-fold for the slowest charge recombination component in moving from solution to the solid state. These studies demonstrate that (1) supramolecular polymer structure can be translated from solution to the solid state, resulting in hierarchical films, and (2) photophysical properties can be enhanced as a result of long-range ordering. The approach to designing new photoactive films demonstrated herein, where hierarchical structure and photophysics are considered synergistically, could provide new strategies for sensing, energy harvesting, and molecular computing.

■ ASSOCIATED CONTENT

Supporting Information

The Supporting Information is available free of charge on the ACS Publications website at DOI: 10.1021/acs.jpcc.5b03713.

Crystal structures, film preparation, and characterization using solid state NMR, AFM, GIWAXS, SEM, and

optical spectroscopy including transient absorption spectroscopy and kinetics (PDF)

■ AUTHOR INFORMATION

Corresponding Authors

*E-mail: amscott@miami.edu.

*E-mail: a.braunschweig@miami.edu.

Notes

The authors declare no competing financial interest.

■ ACKNOWLEDGMENTS

This work was supported in part by grants from the University of Miami, Army Research Office (W911NF-14-1-0164), and a National Science Foundation Graduate Research Fellowship to C.X.G. Financial support from Arizona State University and San Diego State University, Department of Defense Air Force Office of Scientific Research (DOD-AFOSR) (FA9550-14-1-0014), the Defense University Research Instrumentation Program (DURIP) (FA2386-12-1-3031) DURIP 12RSL231 CHESS is supported by the NSF & NIH/NIGMS via NSF award (DMR-0936384)

■ REFERENCES

- (1) Sun, Y.; Welch, G. C.; Leong, W. L.; Takacs, C. J.; Bazan, G. C.; Heeger, A. J. Solution-Processed Small-Molecule Solar Cell with 6.7% Efficiency. *Nat. Mater.* **2012**, *11*, 44.
- (2) van der Poll, T. S.; Love, J. A.; Nguyen, T. Q.; Bazan, G. C. Non-Basic High-Performance Molecules for Solution-Processed Organic Solar Cells. *Adv. Mater.* **2012**, *24*, 3646–3649.
- (3) Kyaw, A. K.; Wang, D. H.; Wynands, D.; Zhang, J.; Nguyen, T. Q.; Bazan, G. C.; Heeger, A. J. Improved Light Harvesting and Improved Efficiency by Insertion of an Optical Spacer (ZnO) in Solution-Processed Small-Molecule Solar Cells. *Nano Lett.* **2013**, *13*, 3796–3801.
- (4) Zhong, Y.; Kumar, B.; Oh, S.; Trinh, M. T.; Wu, Y.; Elbert, K.; Li, P.; Zhu, X.; Xiao, S.; Ng, F.; et al. Helical Ribbons for Molecular Electronics. *J. Am. Chem. Soc.* **2014**, *136*, 8122–8130.
- (5) Wasielewski, M. R. Photoinduced Electron-Transfer in Supramolecular Systems for Artificial Photosynthesis. *Chem. Rev.* **1992**, *92*, 435–461.
- (6) Kobori, Y.; Yamauchi, S.; Akiyama, K.; Tero-Kubota, S.; Imahori, H.; Fukuzumi, S.; Norris, J. R. Primary Charge-Recombination in an Artificial Photosynthetic Reaction Center. *Proc. Natl. Acad. Sci. U. S. A.* **2005**, *102*, 10017–10022.
- (7) Scott, A. M.; Miura, T.; Ricks, A. B.; Dance, Z. E. X.; Giacobbe, E. M.; Colvin, M. T.; Wasielewski, M. R. Spin-Selective Charge Transport Pathways through P-Oligophenylene-Linked Donor-Bridge-Acceptor Molecules. *J. Am. Chem. Soc.* **2009**, *131*, 17655–17666.
- (8) Rao, A.; Chow, P. C. Y.; Gelin, S.; Schlenker, C. W.; Li, C. Z.; Yip, H. L.; Jen, A. K. Y.; Ginger, D. S.; Friend, R. H. The Role of Spin in the Kinetic Control of Recombination in Organic Photovoltaics. *Nature* **2013**, *500*, 435–439.
- (9) Gust, D.; Moore, T. A.; Moore, A. L. Mimicking Photosynthetic Solar Energy Transduction. *Acc. Chem. Res.* **2001**, *34*, 40–48.
- (10) Schuster, D. I.; Cheng, P.; Jarowski, P. D.; Guldi, D. M.; Luo, C.; Echegoyen, L.; Pyo, S.; Holzwarth, A. R.; Braslavsky, S. E.; Williams, R. M.; et al. Design, Synthesis, and Photophysical Studies of a Porphyrin-Fullerene Dyad with Parachute Topology; Charge Recombination in the Marcus Inverted Region. *J. Am. Chem. Soc.* **2004**, *126*, 7257–7270.
- (11) Hammarström, L. Artificial Photosynthesis and Solar Fuels. *Acc. Chem. Res.* **2009**, *42*, 1859–1860.
- (12) Ramanan, C.; Smeigh, A. L.; Anthony, J. E.; Marks, T. J.; Wasielewski, M. R. Competition between Singlet Fission and Charge Separation in Solution-Processed Blend Films of 6,13-Bis-(Triisopropylsilyl)ethynyl)Pentacene with Sterically-Encumbered Per-

- ylene-3,4,9,10-Bis(Dicarboximide)S. *J. Am. Chem. Soc.* **2012**, *134*, 386–397.
- (13) Credginton, D.; Jamieson, F. C.; Walker, B.; Nguyen, T. Q.; Durrant, J. R. Quantification of Geminate and Non-Geminate Recombination Losses within a Solution-Processed Small-Molecule Bulk Heterojunction Solar Cell. *Adv. Mater.* **2012**, *24*, 2135–2141.
- (14) Wojtecki, R. J.; Meador, M. A.; Rowan, S. J. Using the Dynamic Bond to Access Macroscopically Responsive Structurally Dynamic Polymers. *Nat. Mater.* **2011**, *10*, 14–27.
- (15) Yan, X.; Wang, F.; Zheng, B.; Huang, F. Stimuli-Responsive Supramolecular Polymeric Materials. *Chem. Soc. Rev.* **2012**, *41*, 6042–6065.
- (16) De Greef, T. F.; Smulders, M. M.; Wolfs, M.; Schenning, A. P.; Sijbesma, R. P.; Meijer, E. W. Supramolecular Polymerization. *Chem. Rev.* **2009**, *109*, 5687–5754.
- (17) Burattini, S.; Greenland, B. W.; Merino, D. H.; Weng, W.; Seppala, J.; Colquhoun, H. M.; Hayes, W.; Mackay, M. E.; Hamley, I. W.; Rowan, S. J. A Healable Supramolecular Polymer Blend Based on Aromatic Pi-Pi Stacking and Hydrogen-Bonding Interactions. *J. Am. Chem. Soc.* **2010**, *132*, 12051–12058.
- (18) Romulus, J.; Henssler, J. T.; Weck, M. Postpolymerization Modification of Block Copolymers. *Macromolecules* **2014**, *47*, 5437.
- (19) Zhang, X.; Whitten, D. G. Preface to the Supramolecular Chemistry at Interfaces Special Issue. *Langmuir* **2011**, *27*, 1245.
- (20) Greenfield, S. R.; Wasielewski, M. R. Excitation Energy Transfer and Charge Separation in the Isolated Photosystem II Reaction Center. *Photosynth. Res.* **1996**, *48*, 83–97.
- (21) Marcos Ramos, A.; Meskers, S. C.; Beckers, E. H.; Prince, R. B.; Brunsveld, L.; Janssen, R. A. Supramolecular Control over Donor-Acceptor Photoinduced Charge Separation. *J. Am. Chem. Soc.* **2004**, *126*, 9630–9644.
- (22) Lefler, K. M.; Co, D. T.; Wasielewski, M. R. Self-Assembly-Induced Ultrafast Photodrivn Charge Separation in Perylene-3,4-Dicarboximide-Based Hydrogen-Bonded Foldamers. *J. Phys. Chem. Lett.* **2012**, *3*, 3798–3805.
- (23) Peeters, E.; van Hal, P. A.; Meskers, S. C.; Janssen, R. A.; Meijer, E. W. Photoinduced Electron Transfer in a Mesogenic Donor-Acceptor-Donor System. *Chem. - Eur. J.* **2002**, *8*, 4470–4474.
- (24) Hartnett, P. E.; Dyar, S. M.; Margulies, E. A.; Shoer, L. E.; Cook, A. W.; Eaton, S. W.; Marks, T. J.; Wasielewski, M. R. Long-Lived Charge Carrier Generation in Ordered Films of a Covalent Perylenediimide–Diketopyrrolopyrrole–Perylenediimide Molecule. *Chem. Sci.* **2015**, *6*, 402–411.
- (25) Wurthner, F.; Chen, Z.; Hoeben, F. J. M.; Osswald, P.; You, C. C.; Jonkheijm, P.; Herrikhuizen, J.; Schenning, A. P. H. J.; van der Schoot, P. A. M.; Meijer, E. W.; et al. Supramolecular P-N-Heterojunctions by Co-Self-Organization of Oligo(P-Phenylene Vinylene) and Perylene Bisimide Dyes. *J. Am. Chem. Soc.* **2004**, *126*, 10611–10618.
- (26) Miller, N. C.; Cho, E.; Junk, M. J.; Gysel, R.; Risko, C.; Kim, D.; Sweetnam, S.; Miller, C. E.; Richter, L. J.; Kline, R. J.; et al. Use of X-Ray Diffraction, Molecular Simulations, and Spectroscopy to Determine the Molecular Packing in a Polymer-Fullerene Bimolecular Crystal. *Adv. Mater.* **2012**, *24*, 6071–6079.
- (27) Jiménez, A. J.; Calderón, R. M. K.; Rodríguez-Morgade, M. S.; Guldi, D. M.; Torres, T. Synthesis, Characterization and Photophysical Properties of a Melamine-Mediated Hydrogen-Bound Phthalocyanine–Perylenediimide Assembly. *Chem. Sci.* **2013**, *4*, 1064–1074.
- (28) Rieth, S.; Li, Z.; Hinkle, C. E.; Guzman, C. X.; Lee, J. J.; Nehme, S. I.; Braunschweig, A. B. Superstructures of Diketopyrrolopyrrole Donors and Perylenediimide Acceptors Formed by Hydrogen-Bonding and $\pi\cdots\pi$ Stacking. *J. Phys. Chem. C* **2013**, *117*, 11347–11356.
- (29) Ley, D.; Guzman, C. X.; Adolfsson, K. H.; Scott, A. M.; Braunschweig, A. B. Cooperatively Assembling Donor-Acceptor Superstructures Direct Energy into an Emergent Charge Separated State. *J. Am. Chem. Soc.* **2014**, *136*, 7809–7812.
- (30) Kang, S. J.; Kim, J. B.; Chiu, C. Y.; Ahn, S.; Schiros, T.; Lee, S. S.; Yager, K. G.; Toney, M. F.; Loo, Y. L.; Nuckolls, C. A. Supramolecular Complex in Small-Molecule Solar Cells Based on Contorted Aromatic Molecules. *Angew. Chem., Int. Ed.* **2012**, *51*, 8594–8597.
- (31) Shaller, A. D.; Wang, W.; Gan, H.; Li, A. D. Tunable Molecular Assembly Codes Direct Reaction Pathways. *Angew. Chem., Int. Ed.* **2008**, *47*, 7705–7709.
- (32) Shahaar, C.; Baram, J.; Tidhar, Y.; Weissman, H.; Cohen, S. R.; Pinkas, I.; Rybtchinski, B. Self-Assembly of Light-Harvesting Crystalline Nanosheets in Aqueous Media. *ACS Nano* **2013**, *7*, 3547–3556.
- (33) Shoaee, S.; Clarke, T. M.; Huang, C.; Barlow, S.; Marder, S. R.; Heeney, M.; McCulloch, I.; Durrant, J. R. Acceptor Energy Level Control of Charge Photogeneration in Organic Donor/Acceptor Blends. *J. Am. Chem. Soc.* **2010**, *132*, 12919–12926.
- (34) Tamayo, A. B.; Tantiwivat, M.; Walker, B.; Nguyen, T. Q. Design, Synthesis, and Self-Assembly of Oligothiophene Derivatives with a Diketopyrrolopyrrole Core. *J. Phys. Chem. C* **2008**, *112*, 15543–15552.
- (35) Ky Hirschberg, J. H.; Brunsveld, L.; Ramzi, A.; Vekemans, J. A. J. M.; Sijbesma, R. P.; Meijer, E. W. Helical Self-Assembled Polymers from Cooperative Stacking of Hydrogen-Bonded Pairs. *Nature* **2000**, *407*, 167–170.
- (36) Schwartz, E.; Palermo, V.; Finlayson, C. E.; Huang, Y. S.; Otten, M. B.; Liscio, A.; Trapani, S.; Gonzalez-Valls, I.; Brocorens, P.; Cornelissen, J. J.; et al. "Helter-Skelter-Like" Perylene Polyisocyanopeptides. *Chem. - Eur. J.* **2009**, *15*, 2536–2547.
- (37) Brunsveld, L.; Meijer, E. W.; Rowan, A. E.; Nolte, R. J. M. Chiral Discotic Molecules: Expression and Amplification of Chirality. *Materials-Chirality* **2004**, *24*, 373–423.
- (38) Chen, P.-Y.; McKittrick, J.; Meyers, M. A. Biological Materials: Functional Adaptations and Bioinspired Designs. *Prog. Mater. Sci.* **2012**, *57*, 1492–1704.
- (39) England, G.; Kolle, M.; Kim, P.; Khan, M.; Munoz, P.; Mazur, E.; Aizenberg, J. Bioinspired Micrograting Arrays Mimicking the Reverse Color Diffraction Elements Evolved by the Butterfly Pierella Luna. *Proc. Natl. Acad. Sci. U. S. A.* **2014**, *111*, 15630–15634.
- (40) Waite, J. H.; Lichtenegger, H. C.; Stucky, G. D.; Hansma, P. Exploring Molecular and Mechanical Gradients in Structural Bioscaffolds. *Biochemistry* **2004**, *43*, 7653–7662.
- (41) Zhang, X.; Richter, L. J.; DeLongchamp, D. M.; Kline, R. J.; Hammond, M. R.; McCulloch, I.; Heeney, M.; Ashraf, R. S.; Smith, J. N.; Anthopoulos, T. D.; et al. Molecular Packing of High-Mobility Diketopyrrolopyrrole Polymer Semiconductors with Branched Alkyl Side Chains. *J. Am. Chem. Soc.* **2011**, *133*, 15073–15084.
- (42) Schmidt, R.; Oh, J. H.; Sun, Y. M.; Deppisch, M.; Krause, A. M.; Radacki, K.; Braunschweig, H.; Konemann, M.; Erk, P.; Bao, Z.; et al. High-Performance Air-Stable N-Channel Organic Thin Film Transistors Based on Halogenated Perylene Bisimide Semiconductors. *J. Am. Chem. Soc.* **2009**, *131*, 6215–6228.
- (43) Eaton, S. W.; Shoer, L. E.; Karlen, S. D.; Dyar, S. M.; Margulies, E. A.; Veldkamp, B. S.; Ramanan, C.; Hartzler, D. A.; Savikhin, S.; Marks, T. J.; et al. Singlet Exciton Fission in Polycrystalline Thin Films of a Slip-Stacked Perylenediimide. *J. Am. Chem. Soc.* **2013**, *135*, 14701–14712.
- (44) Gelinias, S.; Rao, A.; Kumar, A.; Smith, S. L.; Chin, A. W.; Clark, J.; van der Poll, T. S.; Bazan, G. C.; Friend, R. H. Ultrafast Long-Range Charge Separation in Organic Semiconductor Photovoltaic Diodes. *Science* **2014**, *343*, 512–516.
- (45) Beckers, E. H. A.; Chen, Z. J.; Meskers, S. C. J.; Jonkheijm, P.; Schenning, A. P. H. J.; Li, X. Q.; Osswald, P.; Wurthner, F.; Janssen, R. A. J. The Importance of Nanoscopic Ordering on the Kinetics of Photoinduced Charge Transfer in Aggregated Pi-Conjugated Hydrogen-Bonded Donor-Acceptor Systems. *J. Phys. Chem. B* **2006**, *110*, 16967–16978.
- (46) Gregg, B. A. Entropy of Charge Separation in Organic Photovoltaic Cells: The Benefit of Higher Dimensionality. *J. Phys. Chem. Lett.* **2011**, *2*, 3013–3015.